

Bluff Body Flow Separation Control using Surface Dielectric Barrier Discharges

H. Do^{*}, W. Kim[†], M. G. Mungal[‡] and M. A. Cappelli[§]

Mechanical Engineering Department, Stanford University, Stanford CA 94305-3032

Surface dielectric barrier discharges (DBDs) are used to delay flow separation behind a bluff body in atmospheric pressure air. The bluff body is made by connecting a flat plate to a half cylinder tangentially as a round-cornered trailing edge. Four DBD plasma actuators are attached along the surface of the half cylinder. Particle Image Velocimetry (PIV) is utilized for studying the velocity field of the flow. In the first part of the study, flow alteration effects of two different discharge sources – a conventional alternating current (AC) discharge and an ultra short repetitively pulsed plasma discharge (USRD) - are compared for identical surface DBD configurations. It is found that, at an identical discharge power (~ 25 W), the AC discharge shows higher ability for flow alteration than the USRD. In the second part, the flow alteration effect of the AC DBD is investigated for varying free stream flow speeds, surface roughness, Reynolds number (Re_x), and electrode configuration. The flow speed ranges from 10 m/s to 25 m/s and the corresponding Re_x are from $5 \times 10^4 - 5 \times 10^5$. In this flow regime, the separation point behind the bluff body can be moved downstream in the presence of the AC DBD. However, it is found that, as the flow speed increases, the separation delay effect decreases. The flow alteration effect also decreases with rougher surfaces and higher Re_x . Finally, skewed electrodes and reversed electrodes relative to the flow direction are utilized as two different electrode configurations. It is seen that the skewed electrode provides a positive effect on separation delay while the reversed electrode induces earlier flow separation.

I. Introduction

Active flow separation control techniques have been studied to improve aerodynamic performance of moving objects in fluids such as aircrafts, motor vehicles and turbine blades. Most of the flow actuation techniques are concentrated on the reattachment of separated flow which results in enhancing lift and/or reducing drag forces. Flow reattachment can be achieved using surface blowing to construct a pseudo streamline-shaped surface, surface suction to obtain a thinner boundary layer, vortex generation to increase flow stability, and synthetic jets to utilize the effects of momentum injection into a boundary layer¹⁻³. However, these techniques require an added complexity to the system and offer limited controllability in eliminating or delaying flow separation. Recently, the use of plasma discharges has been proposed as an alternative method to control flow separation. This is because a plasma discharge can generate high energy ions in the vicinity of electrodes which introduce a body force due to the presence of the persisting electric field. This additional body force resulting from the strong directional ion flow can suppress flow separation as it can be used to overcome the destabilizing adverse pressure gradient. The only drawback of such plasma actuators is that they require a high voltage power supply, unlike some of the other passive flow separation control methods mentioned earlier.

^{*} Graduate Research Assistant, Mechanical Engineering, AIAA Student Member.

[†] Post Doctoral Researcher, Mechanical Engineering, AIAA Student Member.

[‡] Professor, Mechanical Engineering, AIAA Associate Fellow.

[§] Professor, Mechanical Engineering, AIAA Member.

A key feature of plasma actuation is the use of nonequilibrium (non-thermal) plasma discharges. Such discharges have received considerable attention because of their relatively low power consumption yet high degree of ion generation. At sufficiently high values of electric field to gas density ratio (E/n), thermal heating of the surrounding gas is minimized, and the nonequilibrium discharge can efficiently target the energy deposition into electron impact and associative ionization of target molecules. A now common method of achieving nonequilibrium discharges at high (i.e., ambient) air pressure is the surface-mounted dielectric barrier discharge (DBD). In prior studies, surface DBDs have been applied to the stabilization of boundary layers on a flat plate configuration⁴⁻⁹, to reduce skin friction on flat pannels⁴, and to alter the flow separation behind bluff bodies such as cylinders^{10, 11} and airfoils^{12, 13}. The velocity range investigated in most of these prior studies is from 0 to 15 m/s. Higher velocity ranges have been investigated for flow actuation at the leading edge of a wing^{12, 13} or on a cylinder using a DC plasma discharge¹⁴. The electrode configurations and discharge operating conditions were varied with the choice of bluff body shapes or velocity range.

The study described here further investigates nonequilibrium plasma-aided flow control and differs from the prior literature in three respects: (i) the geometry of the bluff body considered, (ii) the range of velocity examined, and (iii) the type of applied discharge and its electrode configuration. The bluff body geometry considered here is a cylinder with a tangentially protruding plate, originally designed to mimic the back corner of transportation vehicle such as a large scale truck. The detailed shape is described in the next section below. Such a shape leads to the formation of a much thicker boundary layer prior to encountering the adverse pressure gradient, and hence a much more aggressive environment for flow control, especially at the higher range of flow velocities considered (25 m/s). Such a regime is worthy of investigation since many industrial applications are operated in this range of velocities. Also, the more aggressive flow conditions can provide general ideas on the major control parameters which affect the capability limit of plasma actuators. Here, we test and compare the flow control capabilities of conventional alternating current (AC) DBDs and ultra short repetitively pulsed plasma discharges (USRD). The comparison was motivated by evidence that a USRD generates a more highly nonequilibrium discharge when compared to the AC DBD¹⁵⁻¹⁹. Based on further comparisons carried out here, we have performed more detailed parametric studies of varying velocity, surface roughness, Reynolds number and electrode configuration using AC DBDs, which have proven to be more effective in this particular application.

II. Experimental Setup

The experimental facility used in this study is illustrated in Fig. 1. The setup consists largely of 3 parts - the wind tunnel, the bluff body and plasma source, and the PIV diagnostic system. Two different wind tunnels are used, depending on the velocity range considered. One (30 cm \times 30 cm cross section) is for low flow speed conditions, with operating flow speed of approximately 7.5 m/s. The other (1 m \times 1 m cross section) is for higher flow speed conditions, with an operating range of 10 m/s to 25 m/s.

The shape of the bluff body, and the configuration and alignment of each electrode pair are shown in Fig. 2. The bluff body is made by connecting a flat plate to the tangent of a half cylinder, with the flat plate oriented to be parallel to the free stream flow. Boundary layer development begins at the leading edge of the 20 cm wide flat plate. The length of the flat plate varies from 20 cm to 60 cm. The flow starts to turn its direction along the surface of the 11.4 cm (4.5 inch) diameter ceramic half cylinder until it is separated from the surface. Four electrode pairs are attached along the surface of the half cylinder. Each pair consists of two electrodes: one electrode is exposed to the flow and the other is buried under the dielectric barrier. The exposed electrode is made of 5 mm wide, 0.1 mm thick copper tape. The other electrode is also made of copper tape, however the width of this buried electrode (10 mm) is wider than the exposed electrode to enlarge the area covered by the discharge. This staggered electrode configuration assists to prevent an excessive local electron density which can lead to spark transitions and melting of the dielectric barrier. The width of the discharge is 30 mm. It is noteworthy that a discharge width longer than 30 mm causes a significant voltage drop along the electrode in the

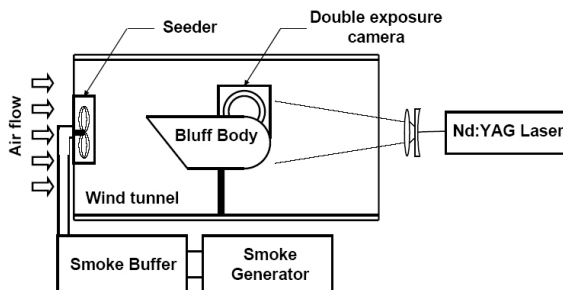


Figure 1. Schematic of experimental setup.

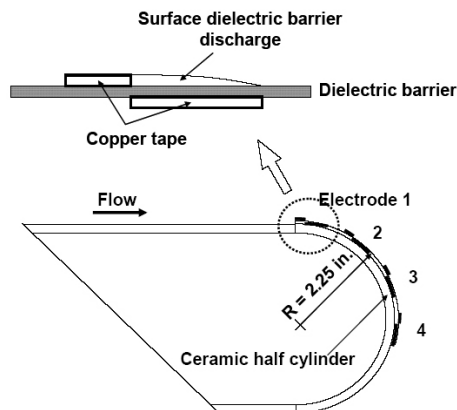


Figure 2. Schematic of the electrode configuration and the bluff body.

current configuration. While the first electrode pair is located at the contact line of the flat plate and the half cylinder (Electrode 1), the last electrode pair is located at 90 degrees along the circumferential direction of the half cylinder (Electrode 4). The second and third electrode pairs (Electrode 2 and 3) are placed between them with equal separation between electrode pairs (30°). The USRD is driven by a power supply capable of producing 6 kV peak voltage pulses, 30 ns in width, at a pulse repetition rate of 40 kHz. Two AC power supplies (Information Unlimited, PVM 300) are used to generate the AC discharges so that each one independently drives two surface discharges. No attempts were made to control the relative phase of these two supplies. The maximum open circuit voltage of these AC power supplies is 20 kV and the range of AC frequency is 20 to 35 kHz. The operation voltage and frequency used in this study are 12 kV peak-to-peak and 25 kHz, respectively. The discharge power is determined from the measured current and voltage using a Rogowski coil (Pearson Electronics, Model 2877) and a 1000:1 high voltage probe (Tektronix,

P6015A), respectively. The signals are collected and stored on a fast digital oscilloscope (Tektronix, TDS 5032B).

For the PIV measurements, a glycerol fog generator (Rosco 1500) and a smoke buffer chamber are used to seed particles into the wind tunnels. The smoke buffer device is used to maintain uniform seeding density in the wind tunnel. The seeder in the wind tunnel pushes smoke into the wind tunnel via an $80\text{ mm} \times 80\text{ mm}$ square fan. Two different laser and camera systems are utilized for convenience. The PIV system for the smaller wind tunnel consists of a Nd:YAG laser (Spectra Physics, PIV-400) and a double exposure camera (KODAK, ES 1.0) while a Nd:YAG laser (New Wave, Gemini PIV) and a double exposure camera (La Vision, Imager Intense) are used for the larger wind tunnel. The 532 nm laser beam emitted from the Nd:YAG laser is formed into a 0.2 mm thick and 5 cm wide sheet via a pair of cylindrical and spherical lenses. Mie scattering between the fog and the laser light are detected by the double exposure camera. The velocity vector field is obtained from two instantaneous sequential images taken with an adjusted time delay. Synchronization of laser shots and the camera is obtained by a delay generator (SRS, DG535), an integrated computer system, and DaVis and PIV 2000 software packages.

III. Results

A. Comparison of USRD and AC DBD

PIV results of flow field obtained from an average of 100 instantaneous images under no discharge, USRD ($\sim 40\text{ kHz}$, $\sim 6\text{ kV}$ peak, $\sim 30\text{ ns}$ pulse width) and AC DBD ($\sim 25\text{ kHz}$, $\sim 12\text{ kV}$ peak to peak) are shown in Figs. 3a, 3b, and 3c, respectively. The measurement was conducted in the low speed wind tunnel which has 7.5 m/s free stream velocity. Flow direction is from the left to the right in the image whose physical dimension is $4.5\text{ cm} \times 4.5\text{ cm}$. Identical electrode configurations are used for the USRD and the AC DBD cases: one electrode (cathode for USRD) is exposed to the flow and the other one (anode for USRD) is buried under the dielectric barrier. It is noteworthy that only two electrode pairs (Electrode 1 at 0° and Electrode 2 at 30°) are active for this experiment. However, the locations of the active electrodes are carefully selected so that the separation point in the absence of the discharge is located between them. A color map is applied to illustrate the vertical velocity profile: blue colors indicate upward vertical velocity regions while red colors depict downward vertical velocity regions. The magnitude and direction of the small blue arrows represent the locally averaged magnitude and direction of the flow velocity, respectively. It is noteworthy that the power dissipated by both discharges is the same (approximately 25 W), even though the peak voltages and frequencies of USRD and AC DBD are not equal.

As seen in the no-discharge case (Fig. 3a), the flow enters the cylinder region with negligible vertical velocity (yellowish green in Region A), starts to bend (dark red) initially along the surface of the cylinder. However, the flow tends to be separated from the cylinder surface just before the Region B in the figure and it loses the downward velocity so that complete flow separation occurs (blue). In the USRD case, a dramatic difference from the no-discharge case is not observed. However, the detailed comparison of the color code in Region A and A' (near the first electrode) and Region B and B' (just after the flow separation) of Figs. 3a and 3b confirms that there exists

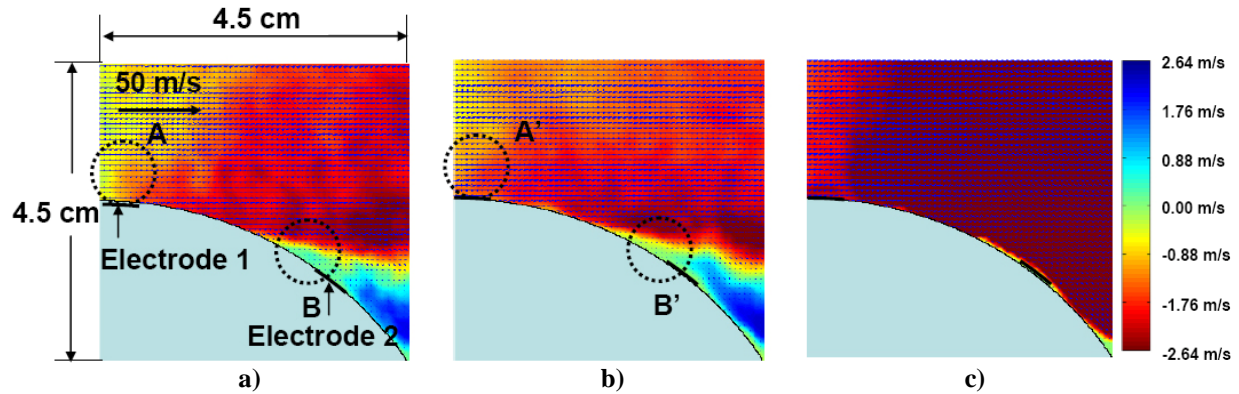


Figure 3. PIV images obtained from an average of 100 instantaneous PIV images near Electrode 1 and 2. Flow speed is 7.5 m/s. The color map illustrates the vertical velocity. a) no discharge, b) 6 kV, 40 kHz USRD, c) 12 kV p-p, 25 kHz AC DBD.

suction flow into the cylinder surface, which supports the influencing effect of the USRD on flow actuation, albeit small. On the other hand, in the presence of the AC DBD (Fig. 3c), there is no blue colored region, which implies that there is much stronger suction flow throughout the entire imaging region. As a result, no flow separation is observed with the AC DBD. In summary, we see that the flow separation is remarkably delayed by the AC DBD, in contrast with only a subtle influence introduced by the USRD.

We believe that the different flow stabilization introduced by the two discharges is mainly due to the difference in the electric field persistence. As mentioned earlier, the flow actuation mechanism can be described by the action of two consecutive processes: ion generation by electron collisions, and directional flow formation by the electric field. Although the USRD is believed to be a more efficient source of ions in comparison to the AC DBD¹⁵⁻¹⁹, its short electric field duration (~ 30 ns) diminishes its flow control ability. We surmise that the ions generated during the discharge pulse are not effectively accelerated between the electrode gap (and hence do not transfer their momentum to the boundary layer fluid) due to the lack of persistence in the electric field. The N_2^+ ion drift velocity in air is ~ 100 m/s at a pressure of 1 atm and voltage of 5 kV over an electrode spacing of 2 mm²⁰. For a typical discharge length of 5 mm along the streamwise direction, the ion residence time in the electrode region is about 50 μ s. This is less than the ion recombination time of several hundred microseconds, which suggests that most ions can survive during the migration time over the electrode should the electric field persist for at least 50 μ s²¹. For the case of the USRD, the typical ion migration distance is only a few micrometers (because of the 30 ns pulse length)-clearly too short to provide significant impact on the boundary layer. In contrast, the AC DBD operating at 25 kHz frequency has its electric field persisting (during a half period) for ~ 20 μ s, resulting in an ion migration distance of ~ 2.5 mm. So it seems that conditions are such that the ions produced by the AC DBD can gain more kinetic energy from the electric field and transfer more momentum into the boundary layer in comparison to the USRD. It is apparent from this simple analysis that the AC DBD should induce a much stronger surface flow.

Figure 4 depicts a typical voltage (red) and current (blue) history for the USRD and the AC DBD. In the case of the USRD (Fig 4a), the very short voltage pulse (~ 30 ns FWHM) and very high peak current (~ 14 A) is confirmed. Significant ringing is observed in both the voltage and current profiles of the USRD, caused by impedance mismatching between the pulse generator and the plasma. In Fig. 4b, the sinusoidal voltage of a period of 40 μ s is seen along with the typical DBD displacement current base (90° phase shift relative to the voltage) and superimposed intermittent current spikes. The peak voltage is approximately 7 kV, comparable to that of the USRD, but the current spikes are distributed around an average of 20 mA, which is significantly lower than the peak current of the USRD. The higher and better defined current profile for the USRD suggests a higher local electron density between the electrodes, i.e., more ion production. However, the shorter electric field duration results in a lesser ability to form a directional ion flow. On the other hand, the AC DBD has a different but effective mechanism to form the ion flow. Since the ions produced by the discharges are mostly positive²², the generation of the ions occurs more frequently when the cathode is the exposed electrode. At this moment, the direction of the electric field is from the buried electrode to the exposed electrode and therefore, most of the ions of positive polarity reside near the exposed electrode. The directional ion drift starts to occur when the electric field reverses: positive polarity on the

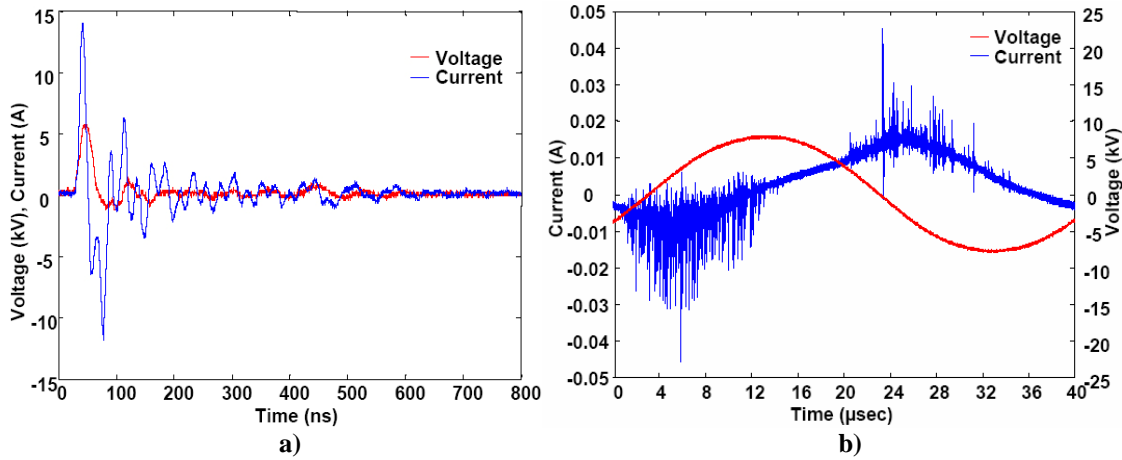


Figure 4. Voltage and current profiles of a) USRD and b) AC DBD.

exposed electrode and negative polarity on the buried electrode. The reversed polarity effectively accelerates the positive ions residing near the exposed electrode resulting in a strong directional flow.

As a result of these findings, we conclude that the AC DBD is a more efficient discharge in comparison to the USRD in its ability to control flow separation. In the following section, the flow actuation performance of the AC DBD will be investigated with varying flow velocities, surface roughness, Reynolds numbers (Re_x) and electrode configurations.

B. Parametric study of the AC DBD

In Fig. 5, vertical (red) and horizontal (blue) flow velocities along the surface of the half cylinder with no discharge (single dot) and AC DBD (double dot) are provided to show the criteria to determine the detailed separation point in the present study. The angle 0 represents the nodal point of the flat plate and the half cylinder while the increase of the angle is measured along the half cylinder surface in the clockwise direction. The free stream velocity is 20 m/s, and the AC DBD is operated at the same frequency and voltage to those conditions of Fig. 3. Throughout this section, we activate all of the four electrode pairs to maximize the flow actuation with the AC DBD. The power consumption of the discharge is twice of that of Fig. 3 (i.e., ~ 50 W). As seen in the figure, we

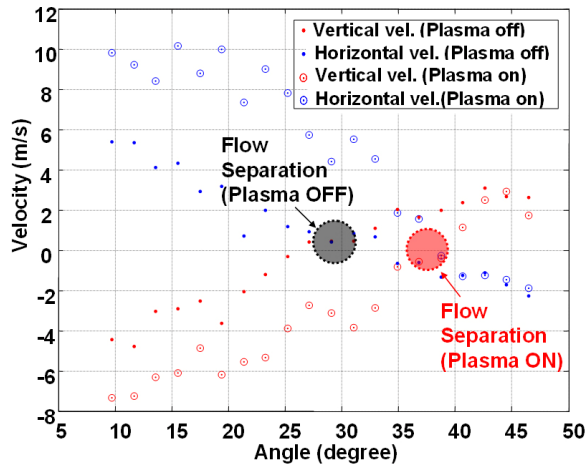


Figure 5. Vertical (red) and horizontal (blue) velocities at points along the surface of half cylinder. The flow speed is 20 m/s. 12 kV p-p voltage and 25 kHz frequency AC DBD is used as a plasma source.

choose the separation point where both vertical and horizontal velocities approach zero. This definition of the separation point is reasonable since the directions of both velocities are reversed after the separation point, implying that a wake exists after this point. With this definition of the separation point, one can better quantify the separation delay which actually occurs with the activated AC DBD. The separation point is just under 30° without the powered AC DBD, but it is delayed to be past 35° with the powered AC DBD. It is noteworthy that, with the powered AC DBD, the horizontal velocities as well as the magnitude of the vertical velocities increase before the flow is separated. This is an important feature since a higher horizontal velocity suggests that the area of wake region behind the bluff body is reduced.

In Fig. 6, PIV images are provided of the flow field obtained from an average of 100 instantaneous PIV images at free stream velocities of 15 m/s (Figs. 6a and 6b), and 20 m/s (Figs. 6c and 6d) to compare the degree of separation delay with varying velocity. Figures 6a and 6c are the base cases (no-discharge) while the others are for the powered

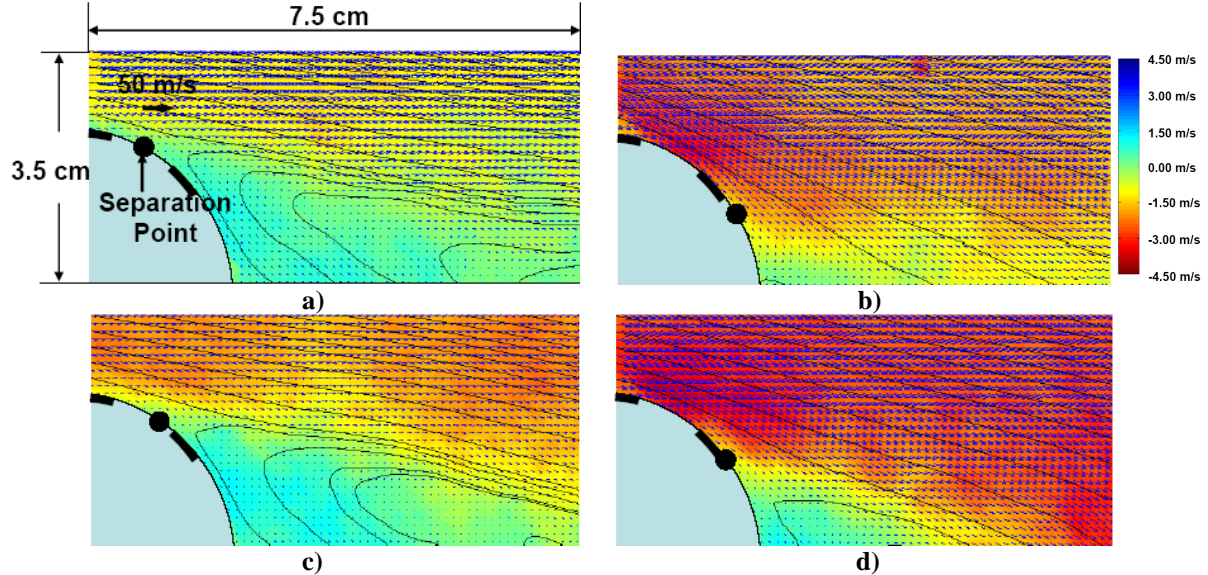


Figure 6. Mean flow field obtained from an average of 100 instantaneous PIV images. a) Without DBD at 15 m/s, b) with DBD at 15 m/s, c) without DBD at 20 m/s and d) with DBD at 20 m/s. The DBD was operated at 12 kV p-p voltage and 25 kHz frequency. Black curves are mean streamlines and the color map illustrates the vertical velocity. The separation points indicated by black dots are moved down stream by the AC DBD.

AC DBD under similar voltage and frequency to the case of Fig. 3. As in Fig. 3, the color code represents the vertical velocity component of the flow. By comparing the separation points illustrated in Figs. 6a and 6c (black dots), one can see that the flow separation point moves downstream with increasing flow speed (even for the non-discharge cases) as expected for the laminar-turbulent transition regime in which the current configuration is ($Re_x \sim 10^5$). In the presence of the powered AC DBD, the separation points move further downstream in both flow speed cases (Figs. 6b and 6d). However, the flow separation delay due to the discharge and resulting flow deflection shown in pseudo streamlines (black curves) in the figure is clearly more enhanced at the lower (15 m/s) flow speed. This is expected for the following two reasons. First, as the flow speed increases, the power deposited by the plasma discharge per molecule (i.e., specific enthalpy) decreases. The lower power/molecule ratio results in a lower average ion density near the discharge, which eventually causes less momentum transfer into the boundary layer. Second, the boundary layer becomes thicker at higher flow speed as the flow becomes more turbulent and therefore, the momentum transfer between the ion drift motion and the boundary layer may become less effective.

We altered the surface roughness of the flat plate and the Re_x to carry out a detailed investigation on the sole effect of boundary layer thickness on flow control. The results are provided in Fig. 7. In this figure, horizontal velocity profiles along a vertical line located at 1 cm downstream from the last electrode are plotted with (red) and without (blue) the powering of the AC DBD. Here, the flow speed is held constant at a value of 15 m/s. The AC DBD is operated at the same condition as before. Figure 7a depicts results for two different surface roughness cases while two different Re_x cases (3.7×10^5 and 5.6×10^5) are shown in Fig. 7b. To increase the surface roughness, ten $10 \text{ mm (width)} \times 5 \text{ mm (height)} \times 5 \text{ mm (thickness)}$ blocks are positioned 5 cm downstream from the leading edge of the flat plate. The Re_x increase (without altering the flow velocity) is achieved by using flat plates of different length (40 cm and 60 cm). It is apparent that the thicker boundary layer due to rougher surface and higher Re_x (curves with circle) decreases the horizontal velocity while an increase in the horizontal velocity is observed with the powered AC DBD for all the four different cases. The reason that a thicker boundary layer interrupts the effect of the discharge seems to be clear: a higher momentum (from the ion drift) is required to control the thicker, therefore, larger amount of slow-moving flow.

Thus far, we have described conditions where the electrode orientations are set to be normal to the flow direction as shown in Fig. 2. This electrode orientation has an advantage in that the AC DBD can induce streamwise flow along the bluff body surface because the direction of the applied electric field is parallel to the flow. However, the

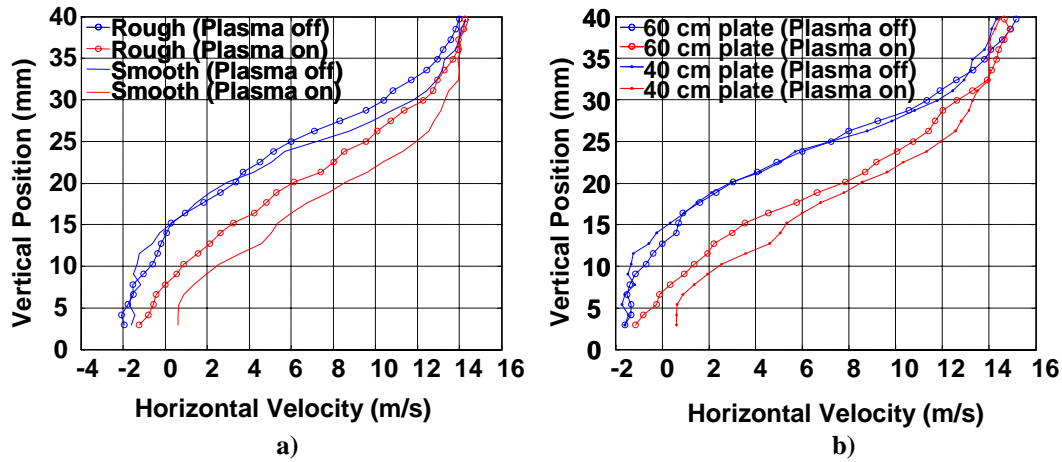


Figure 7. Horizontal velocity profiles along a vertical line located at the 1 cm downstream from the Electrode 4 with varying a) surface roughness and b) Re_x (3.7×10^5 and 5.6×10^5). Free stream flow speed is 15 m/s in both cases. Discharge operation condition is identical to that of Fig. 6.

skewed electrode configuration is worthy of investigation since it can increase the power/molecule ratio with increasing skew angle. For example, when electrodes are placed at 45° relative to the flow direction, the effective width of the surface discharge per unit number of air molecules decreases by a factor of $\cos 45^\circ$. Therefore, the power/volume ratio increases by that amount. The effect of skewed electrodes is shown in Fig. 8, where the flow separation angles are plotted as a function of free stream velocity with no discharge (blue), normal discharge (red) and skewed discharge by 45° (black). The voltage and frequency of the AC DBD are again the same as for the prior results. While the no-discharge case reconfirms the separation delay due to the laminar-turbulent transition with increasing free stream velocity, the skewed electrode configuration shows a better ability to delay the separation point at every flow speed, a feature of practical importance. However, the effect of a skewed electrode decreases with increasing free stream flow speed. We believe that a further investigation is required to obtain a clearer understanding of this phenomenon.

As a final comment, it is interesting to demonstrate conditions of how the direction of the electric field alters the

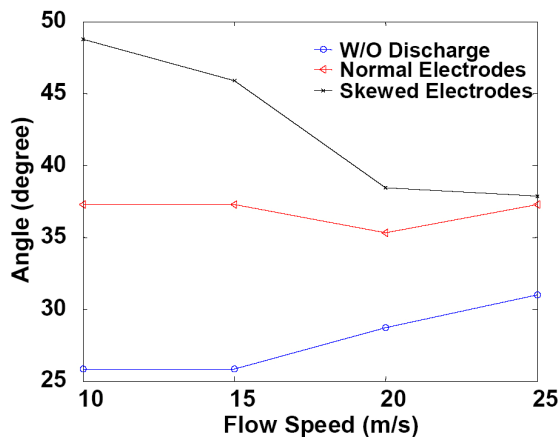


Figure 8. The position (angle) of separation points on the surface of half cylinder. The flow speed varies from 10 m/s to 25 m/s. Two different electrode configurations are used which are normal and skewed by 45 degree angle to the flow direction. Discharge operation condition is identical to that of Fig. 6.

flow separation point¹¹. To investigate this, we tested two electrodes configurations – the usual case that produces a streamwise body force, and a reverse configuration to produce an opposing body force, as shown in Figs. 9a and 9b, respectively. A reverse electric field can be achieved by placing the buried electrode upstream of the exposed electrode. The PIV images of the flow field obtained from an average of 100 instantaneous PIV images are shown in Figs. 9c and 9d. These images are obtained for a condition of 15 m/s free stream velocity. From the pseudo streamlines (red curves) and separation point (black dot), one can see the entire flow becomes unstable with the reverse electrode (Fig. 9d) in comparison to with the forward electrode (Fig. 9c). For reference, the separation point of the reverse electrode configuration is outside of the imaging region. This augmented instability is due to the fact that the applied electric field is directed upstream, therefore, the ion motion is also directed upstream. Consequently, the flow induced by the AC DBD forms a counter stream to the main flow, which causes surface blowing and assists the flow in separated from the

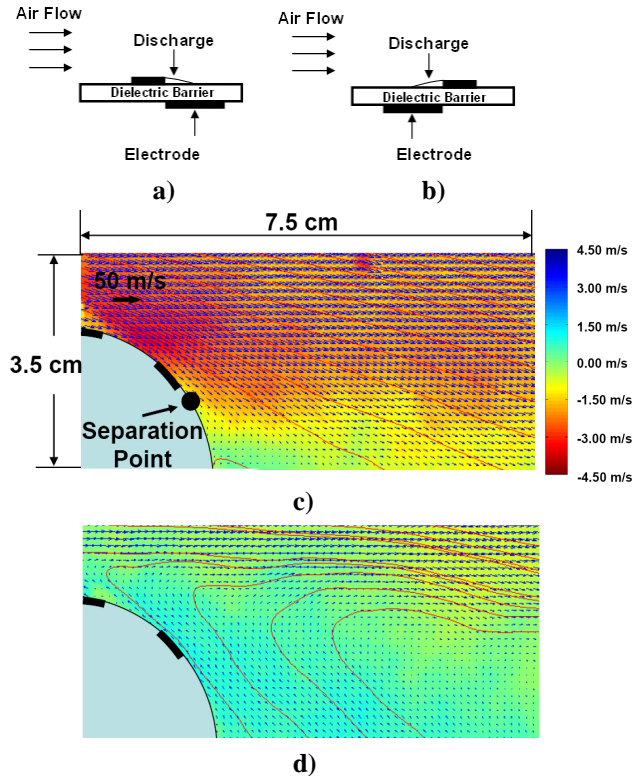


Figure 9. Schematics of electrode configurations. a) Forward electrode configuration and b) reversed electrode configuration. PIV images obtained from an average of 100 instantaneous PIV images. c) With forward electrode configuration and d) with reversed electrode configuration. The flow speed is 15 m/s. Discharge operation condition is identical to that of Fig. 6. Red curves are the streamlines and the color map illustrates the vertical velocity.

Reynolds number (Re_x), and electrode configuration. As a result, we concluded that higher free stream speed and thicker boundary layer due to rougher surfaces and higher Re_x weaken the flow alteration effect. At a higher free stream speed condition, the power deposition by the discharge per unit number of air molecules decreases, which results in lower ion density and less momentum transfer into the boundary layer. Furthermore, the thicker boundary layer makes momentum transfer between the ion flows and boundary layer less effective. Finally, the effect of different electrode configurations, skewed and reversed electrode, was investigated. With the skewed electrode configuration, it was found that the flow separation can be delayed further due to higher power/molecule ratio while the AC DBD with a reversed electrode configuration promotes flow separation. This result confirms the possibility of plasma aided flow actuators which are able to generate blowing as well as suction surface flows.

References

- ¹Culley, D. E., Bright, M. M., Prahst, P. S., and Strazisar, A. J., "Active Flow Separation Control of a Stator Vane Using Surface Injection in a Multistage Compressor Experiment," NASA, TM-2003-212356, 2003.
- ²Kim, S. H., and Kim, C., "Separation Control on NACA23012 Using Synthetic Jet," *3rd AIAA Flow Control Conference*, San Francisco, 2006, AIAA 2006-2853.

surface at an earlier point. Clearly, the AC DBD actuation can be used to separate flow from the surface as well as to reattach flow to the surface. This further confirms that the flow actuation is not thermally induced by the discharge but results from the ion motion powered by the electric field between the electrodes¹¹.

IV. Conclusion

The present study consisted of two parts: the first part was the comparison of flow actuation using an ultra short repetitively pulsed plasma discharge (USRD) and an alternating current dielectric barrier discharge (AC DBD). AC (~ 12 kV peak-to-peak, ~ 25 kHz) and USRD (~ 6 kV peak, ~ 40 kHz, ~ 30 ns pulse width) of similar powers (~ 25 W) were used with an identical surface electrode configuration. It was found that the AC DBD has a better ability to delaying separation than the USRD, while, in comparison to the cases of no discharge, both discharges induce the suction flow which can delay the flow separation. The better performance of the AC DBD is attributed to its persistent electric field (lasting for about $20 \mu\text{s}$) in comparison to that of the USRD (which lasts for about 30 ns). In the presence of the AC DBD, the streamwise momentum flux caused by the ion motion is much stronger than that of the USRD. We note that for flame stabilization applications involving plasmas the USRD is superior owing to the ability to provide high degrees of non-equilibrium¹⁵⁻¹⁹, and hence to produce a region rich in reactive species, but this advantage does not translate to flow control applications.

In the second part of the paper, the flow alteration effect of the AC DBD was investigated by varying free stream flow speed, surface roughness,

- ³Volino, R. J., "Separation Control on Low-Pressure Turbine Airfoils Using Synthetic Vortex Generator Jets," *Journal of Turbomachinery*, 2004, Vol. 125, pp. 765-777.
- ⁴Jukes, T. N., Choi, K., Johnson, G., and Scott, S. J., "Turbulent Boundary-Layer Control for Drag Reduction Using Surface Plasma," *2nd AIAA Flow Control Conference*, Portland, 2004, AIAA-2004-2216.
- ⁵Roth, J. R., and Sherman, D. M., "Electrodynamic Flow Control with a Glow-Discharge Surface Plasma," *AIAA Journal*, Vol. 38, No. 7, 2000, pp. 1166-1172.
- ⁶Enloe, C. L., McLaughlin, T. E., Van Dyken, R. D., Kachner, K. D., Jumper, E. J., Corke, T. C., Post, M., and Haddad, O., "Mechanisms and Responses of a Single Dielectric Barrier Plasma Actuator: Geometric Effects," *AIAA Journal*, Vol. 42, No. 3, 2004, pp. 595-604.
- ⁷Enloe, C. L., McLaughlin, T. E., Van Dyken, R. D., and Kachner, K. D., "Mechanisms and Response of a Single Dielectric Barrier Plasma Actuator: Plasma Morphology," *AIAA Journal*, Vol. 42, No.3, 2004, pp. 589-594.
- ⁸Roth, J. R., and Sherman, D. M., "Boundary Layer Flow Control with a One Atmosphere Uniform Glow Discharge Surface Plasma," *36th AIAA Aerospace Sciences Meeting and Exhibit*, Reno, 1998, AIAA-1998-328.
- ⁹Roth, J. R., "Aerodynamic Flow Acceleration Using Paraelectric and Peristaltic Electrohydrodynamic Effect of a One Atmosphere Uniform Glow Discharge Plasma," *Physics of Plasmas*, Vol. 10, No. 5, 2003, pp. 2117-2126.
- ¹⁰Asghar, A., "On the Use of Reynolds Number as the Scaling Parameter for the Performance of Plasma Actuator in a Weakly Compressible Flow," *44th AIAA Aerospace Sciences Meeting and Exhibit*, Reno, 2006, AIAA-2006-170.
- ¹¹Sung, Y., Kim, W., Mungal, M. G., and Cappelli, M. A., "Aerodynamic Modification of Flow over Bluff Objects by Plasma Actuation," *Experiments in Fluids*, Vol. 41, No. 3, 2006, pp. 479-486.
- ¹²Roupassov, D., Zavialov, I., and Starikovskii, A. Yu., "Boundary Layer Separation Plasma Control Using Low-Temperature Non-Equilibrium Plasma of Gas Discharge," *44th AIAA Aerospace Sciences Meeting and Exhibit*, Reno, 2006, AIAA-2006-373.
- ¹³Post, M. L., and Corke, T. C., "Separation Control on a High Angle of Attack Airfoil Using Plasma Actuators," *AIAA Journal*, Vol. 42, No. 11, 2004, pp. 2177-2184.
- ¹⁴Artana, G., Sosa, R., Moreau, E., and Touchard, G., "Control of the Near-Wake Flow Around a Circular Cylinder with Electrohydrodynamic Actuators," *Experiments in Fluids*, Vol. 35, 2003, pp. 580-588.
- ¹⁵Kim, W., Do, H., Mungal, M. G., and Cappelli, M. A., "Parametric Study of Flame Stabilization and NO Production in a Plasma Assisted Methane/Air Premixed Flame," *WSS/CI Fall Meeting*, Stanford, 2005, 05F-78.
- ¹⁶Kim, W., Mungal, M. G., and Cappelli, M. A., "Flame Stabilization Using a Plasma Discharge in a Lifted Jet Flame," *43rd AIAA Aerospace Sciences Meeting and Exhibit*, Reno, 2005, AIAA-2005-931.
- ¹⁷Kim, W., Do, H., Mungal, M. G., and Cappelli, M. A., "Flame Stabilization Enhancement and NOx Production using Ultra Short Repetitively Pulsed Plasma Discharges," *44th AIAA Aerospace Sciences Meeting and Exhibit*, Reno, 2006, AIAA-2006-560.
- ¹⁸Kim, W., Do, H., Mungal, M. G., and Cappelli, M. A., "Investigation of NO Production and Flame Structure in Plasma Enhanced Premixed Combustion," *Proceedings of the Combustion Institute, 31st International Combustion Symposium*, Heidelberg, 2006 (to be published).
- ¹⁹Kim, W., Do, H., Mungal, M. G., and Cappelli, M. A., "Plasma Discharge Stabilization of Jet Diffusion Flames," *IEEE Transaction on Plasma Sciences*, 2006 (to be published).
- ²⁰Saporoschenko, M., "Mobility of Mass-Analyzed N^+ , N_2^+ , N_3^+ , and N_4^+ Ions in Nitrogen Gas," *Physical Review*, Vol. 139, No. 2A, 1965, pp. A352-A356.
- ²¹McGowan, S., "Ion-Ion Recombination in Laboratory Air," *Phys. Med. Biol.*, Vol. 10, No. 1, 1964, pp. 25-40.
- ²²Fridman, A., Chirokov, A., and Gutsol, A., "Non-Thermal Atmospheric Pressure Discharges," *Journal of Physics D: Applied Physics*, Vol. 38, 2005, pp. R1-R24.